**Wind and Structures**, *Vol. 19, No. 2 (2014) 219-232*
DOI: http://dx.doi.org/10.12989/was.2014.19.2.219 

# Effects of inflow turbulence and slope on turbulent boundary layers over two-dimensional hills

Tong Wang*[1,2], Shuyang Cao[2a] and Yaojun Ge[2b]

[1]*College of Civil Engineering, Shanghai NormalUniversity, Shanghai 201418, China*
[2]*Department of Bridge Engineering, Tongji University, Shanghai 200092, China*

*(Received August 16, 2013, Revised June 20, 2014, Accepted July 6, 2014)*

**Abstract.** The characteristics of turbulent boundary layers over hilly terrain depend strongly on the hill slope and upstream condition, especially inflow turbulence. Numerical simulations are carried out to investigate the neutrally stratified turbulent boundary layer over two-dimensional hills. Two kinds of hill shape, a steep one with stable separation and a low one without stable separation, and two kinds of inflow condition, laminar and turbulent, are considered. An auxiliary simulation, based on the local differential quadrature method and the recycling technique, is performed to simulate the inflow turbulence to be imposed at the inlet boundary of the simulation with turbulent inflow, which preserves very well in the computational domain. A large separation bubble is established on the leeside of the steep hill with laminar inflow, while the reattachment point moves upstream under turbulent inflow condition. There is stable separation on the lee side of the low hill with laminar inflow, while not with turbulent inflow. Besides increase of turbulence intensity, inflow turbulence can efficiently enhance the speedup around hills.So in practice, it is unreasonable to study wind flow over hilly terrain without considering inflow turbulence.

**Keywords:** inflow turbulence; slope; turbulent boundary layer; two-dimensional hill; separation;speedup; numerical simulation

## 1. Introduction

With increased interest in wind energy application and increasing number of factories and wind-sensitive structures in mountainous region, the turbulent atmospheric boundary layer (ABL) over complex terrain has become a hot research topic in the field of wind engineering for the past two decades, especially in China. Identifying positions with accelerations in the mean wind and their magnitudes is crucial for wind turbine siting, whereas changes to both the mean wind and turbulence are important when predicting the dispersion of atmospheric pollutants or estimating the wind load on structures in mountainous region. Turbulent flow over complex terrain involves complicated flow phenomena, such as spatial development, separation and reattachment according to the hill slope, and downstream recovery of turbulent boundary layer. Any disturbance that may influence the behavior of the separated shear layer and its interaction with the ground would

*Corresponding author, Ph. D., E-mail: wangtong.tju@gmail.com
[a] Professor, E-mail: shuyang@tongji.edu.cn
[b] Professor, E-mail: yaojunge@tongji.edu.cn


http://www.techno-press.org/?journal=was&subpage=8 ISSN: 1226-6116 (Print), 1598-6225 (Online)

change the global and local turbulent structure and thus influence the wind characteristics around hilly terrain. The inflow turbulence and slope are two important factors in determining the dynamic behavior of the turbulent boundary layer over hills. Many investigations have studied the turbulent boundary layer over an isolated hill, which is usually a start point in research on flow over complex terrain. Generally, there are three approaches to investigate or predict the flow around hilly terrain. The most used analytical method to handle the effects of inflow turbulence and slope is based on the assumption of a linear superposition of the individual effects of the inflow turbulence and slope (Jackson and Hunt 1975, Hunt *et al.* 1988). However, there is no evidence that these two effects can be treated as completely independent. Mason and King (1985) showed through field measurements that the linear theory failed to predict the extent of the velocity reduction in the lee of a real hill. Wind tunnel experiment is also often used to study the flow over hills. Neff and Meroney (1998) investigated the vegetation influence on wind power availability in terms of amplification of wind speed on a crest with and without vegetation on its surface. Miller and Davenport (1998) examined the Canadian and UK wind loading codes of practice for predicting speedup on the crests of complex terrain considering surrounding topography and surface roughness through experimental measurements. Cao and Tamura (2006, 2007) studied the effects of surface roughness blocks on ABL flow over two-dimensional steep and low hills with/without sudden roughness change. Recently, Ngo and Letchford (2009) experimentally studied the effects of upwind slopes on speedup ratio over ridges with and without carpet. One common conclusion of these experimental studies was the necessity to consider upstream condition and surface roughness when predicting speedup. However, a complex terrain usually requires modeling of an area that is too large to achieve in a wind tunnel. Thus, the numerical approach, which has great potential to play a similar role as the wind tunnel due to the improvement of computational capacity, is considered as an alternative means to predict unsteady turbulent flow around hilly terrain.

Although the Reynolds averaged Navier-Stokes (RANS) equations-based numerical methods are still widely applied in the simulation of flow over complex terrain (for instance, Ishihara and Hibi 2002, Lun *et al.* 2003), Large-eddy simulation (LES) has become an increasingly used method for predicting turbulence structures and statistics because it enables time-dependent calculation of unsteady flows including large-scale vortices, which are usually established in the wake of a steep hill. There have been many reported LES researches that aimed to study aspects of turbulent flow over hills under neutral flow conditions. Hennand Sykes (1999) and Gong *et al.* (1996) carried out LES studies of the separated turbulent flow over wavy smooth and aerodynamically rough two-dimensional sinusoidal surfaces individually. Tamura *et al.* (2007) conducted an LES study of turbulent boundary layers over a smooth and a rough two-dimensional hill with a discussion of the applicability of turbulence models. In our recent work of Cao *et al.* (2012), the effects of surface roughness and slope on turbulent boundary layers over two-dimensional hills were numerically studied. However, as discussed in a review paper of Bitsuamlak *et al.* (2004), the majority of numerical simulations could not yield satisfactory results for speed-up ratio over hills in the presence of flow separation. The necessity of carrying out more studies to improve the accuracy of numerical simulation partly motivated the present study.

As our focus is on the effects of inflow turbulence on the neutrally stratified turbulent boundary layer over two-dimensional hills at different slopes, two representative inflow conditions, i.e., a laminar one and a turbulent one, are considered, as well as two representative hill shapes, i.e., a steep one with stable separation and a low one without stable separation. The results may change

with Reynolds number, i.e., Reynolds number effect. However, this factor is not considered here. The simulation is carried out only at a low Reynolds number around 1100, and for convenience, no turbulence model is considered. Setting of inflow condition for the turbulent inflow case is a key process. As pointed out by Blocken *et al.* (2007), how to impose the inlet velocity boundary conditions and how to maintain the turbulence characteristic inside the computational domain are important. Wang *et al.* (2013) incorporated the local differential quadrature method (DQM) and the recycling technique to simulate the inflow turbulence with the effort to improve the high-frequency component of turbulence. Process of this method and its behavior will be given in Section 2. Section 3 presents calculation details of flow over hills. Section 4 analyzes the influence of inflow turbulence and hill slope on the turbulent boundary layer over hills through comparisons. Finally, some conclusions are summarized in Section 5.

## 2. Generation of inflow turbulence

The methods developed till now to generate inflow turbulence can generally be classified into two types. The first one is the analytical method that artificially generates time series of velocity fluctuations by performing an inverse Fourier transformation-based simulation (Kondo *et al.* 1997). Another is the CFD method that directly conducts numerical simulation of a turbulent boundary layer using CFD approach (Kataoka and Mizuno 2002, Wang *et al.* 2013). The stochastic nature of inflow turbulence generated by the analytical method may satisfy the prescribed requirements of the turbulence statistics at one point or sometimes correlated multiple points. However, as long as it is not generated from the governing equations of the fluid, the velocity fluctuations cannot have the organized structures of a turbulent ABL, thus the wind-induced response of a structure obtained at this kind of "turbulent" flow is questionable. In contrast, the CFD method avoids the problems caused by the analytical method while requires a large computational load. With the CFD method, it is possible to simulate a fully-developed or spatially-developing turbulent boundary layer whose turbulent flow field at one location can be extracted and utilized as the time-dependent inflow data for other calculations. However, the resolution of the flow field is basically dependent on grid size, thus very fine grid is necessary to simulate the high-frequency component of turbulence, which results in a large computational effort. Another approach to increasing the high-frequency component of turbulence is to use high-order algorithms to express the derivative. This paper adopted the method of Wang *et al.* (2013), which applied the high-order local DQM combined with the recycling technique of Kataoka and Mizuno (2002) to generate the inflow data. This method can efficiently enhance the high-frequency energy. Fig. 1 illustrates the basic concept of this method, in which the fluctuating components are directly extracted from a downstream recycling station and introduced at the inlet boundary without rescaling process, assuming the mean velocity profile prescribed at the inlet does not change in the computational domain during the time advancement. Concretely, the velocity components at the inlet are given as follows

$$\begin{cases} u_{\text{inlt}}(y,z,t) = \langle u \rangle_{\text{inlt}}(z) + \varphi(\eta) \times \{u(y,z,t) - \langle u \rangle(y,z)\}_{\text{recy}} \\ v_{\text{inlt}}(y,z,t) = \varphi(\eta) \times \{v(y,z,t) - \langle v \rangle(y,z)\}_{\text{recy}} \\ w_{\text{inlt}}(y,z,t) = \varphi(\eta) \times \{w(y,z,t) - \langle w \rangle(y,z)\}_{\text{recy}} \end{cases} \tag{1}$$

where $u$, $v$, $w$ are the velocity variables along the $x$, $y$, $z$ axis, respectively; $t$ is time; the subscripts

of "inlt" and "recy" denote the values at the inlet and recycling stations, respectively; ⟨⟩ represents a time-averaged value; $\langle u\rangle_{\text{inlt}}$ is the prescribed velocity profile imposed at the inlet boundary; $\varphi(\eta)$ is the damping function that blocks the velocity fluctuation from developing in the free stream; $\eta=y/\delta$ and $\delta$ is the boundary layer thickness. In this paper, we use the damping function shown as Eq. (2), proposed by Kataoka (2008). It should be indicated here that the damping function has a significant influence on the final results as pointed out by Wang *et al.* (2013), and this will also be discussed hereafter.

$$\varphi(\eta)=\frac{1}{2}\left\{1-\tanh\left[\frac{8.0(\eta-1)}{0.2-0.4\eta}\right]/\tanh(8.0)\right\} \tag{2}$$

The governing equations of flow used here are the three-dimensional unsteady incompressible Navier-Stokes equations in Cartesian coordinate. A common staggered mesh is introduced: the pressure $p$ is defined in the center of the cell, and the velocities $u$, $v$, $w$ are defined at the surface center of the cell normal to $x$, $y$, $z$ axis, respectively. The traditional fractional step method is applied to solve these governing equations. And the local DQM shown by Wang *et al.* (2013) is only used to discretize the convection terms in space while calculating the intermediate velocities, and the viscous terms are spatially discretized by the second-order central difference scheme. In time, the first-order explicit Euler scheme is used for the unsteady terms, the second-order Adams-Bashforth scheme for the convection terms and the Crank-Nicolson scheme for the viscous terms.

The simulation of inflow turbulence is usually an auxiliary job to generate the inlet boundary data of a major simulation, thus its computational load must be as less as possible. On the other hand, the Kataoka's method that assumed a constant boundary layer thickness in the computational domain also requests a comparatively short computational domain.In the present study, the streamwise length of the computational domain is $1.5\delta$ and the distance from the inlet to the recycling station is $1.0\delta$ ($\delta$: boundary layer thickness). The computational domain length in the vertical and spanwise direction is $2.5\delta$ and $1.0\delta$ respectively. A relatively coarse mesh is applied, which is 50×110×30 in streamwise, vertical and spanwise directions. The grid space is equal in streamwise and spanwise directions ($\Delta x=\Delta z=0.03\delta$), and unequal in vertical direction. The vertical grid size varies from $0.001\delta$ near the wall to $0.083\delta$ at the ceiling.The CFL number is around 0.23. The damping function of Eq. (2) is used without optimization.

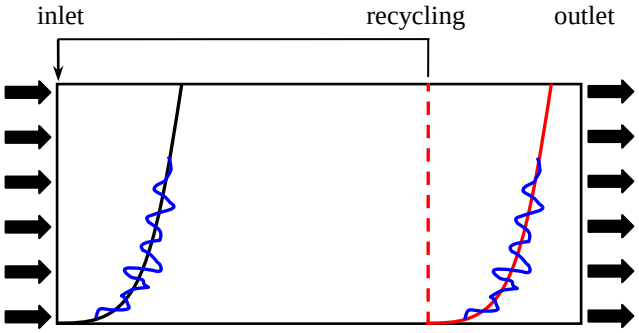


Fig. 1 Concept of Kataoka's recycling method

We simulated the turbulent inflow at $Re_\theta$=1020 based on the momentum thickness. Fig. 2 shows the vertical profile of streamwise mean velocity and corresponding turbulent intensity, compared with experimental results of Degraaff and Eaton (2000) at $Re_\theta$=1430. Clearly, the mean-velocity profile was regenerated very well. However, the turbulence intensity was overestimated within the boundary layer height and underestimated above it. The selected damping function attributes to these results. Besides, taking into account the effect of Reynolds number, it can be concluded that the generated inflow turbulence statistics are in reasonably good agreement with the experimental data. Fig. 3 shows the power spectral densities of the along-wind velocity fluctuation obtained by a low-order scheme (third-order) and a high-order scheme (seventh-order), compared with the Karman spectrum. As shown in the figure, the improvement of the high-frequency energy at the high-order scheme is remarkable.

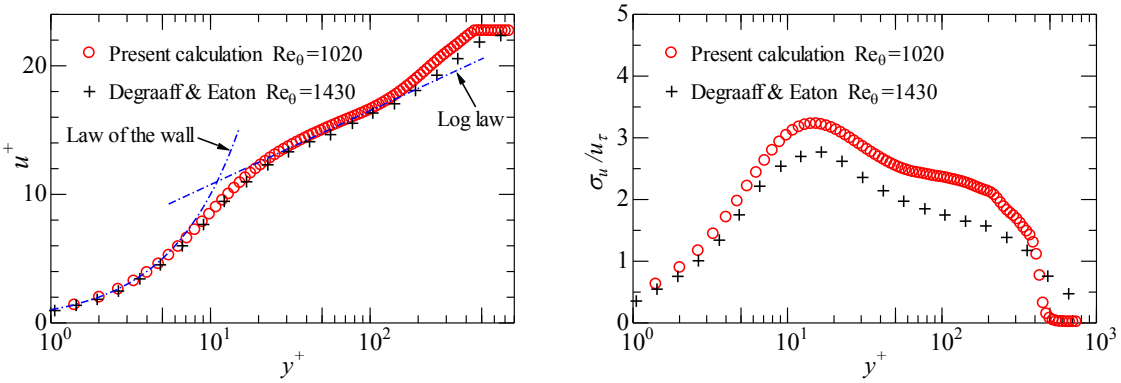


(a) Mean velocity (b) Turbulent intensity

Fig. 2 Statistics of generated inflow data

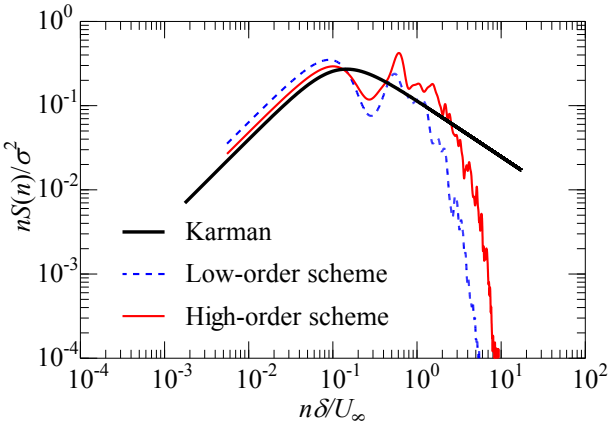


Fig. 3 Calculated power spectral densities with different schemes

## 3. Calculation details of flow over hills

The hill considered has a sinusoidal geometrical shape as defined by

$$y = H\cos^2\left(\frac{\pi x}{2L}\right) \tag{3}$$

where $H$ is the hill height and $L$ is the half hill length, as illustrated in Fig. 4. Two hill shapes are considered, $L$=2.5$H$ and $L$=7.5$H$, with maximum slope angles of 32 degrees and 12 degrees, respectively. The critical angle to establish stable separation in the wake under turbulent upstream condition is roughly 16 degrees (Finnigan 1988), so these two hill shapes correspond to two completely different flow patterns under turbulent inflow condition. Besides, for convenience, only smooth hill surface condition is considered in the present study.

For the turbulent inflow case, the numerical simulation consists of two parts actually, as illustrated in Fig. 5. The main simulation is carried out for the turbulent flow over a hill, while an auxiliary simulation is for the generation of inflow turbulence using the method given in Section 2. Both simulations can be carried out synchronously or asynchronously (asynchronously in the present paper) and the data numerically obtained in the auxiliary simulation are stored and imposed at the inlet boundary of the main simulation at each time step. The generalized curvilinear coordinate system and the Cartesian coordinate system are used to formulate the numerical models for these two simulations respectively. However, for the laminar inflow case, only the main calculation domain in Fig. 5 is used. For comparison, the velocity condition at the inlet boundary is defined as the mean-velocity profile of the inflow data for the turbulent inflow case.

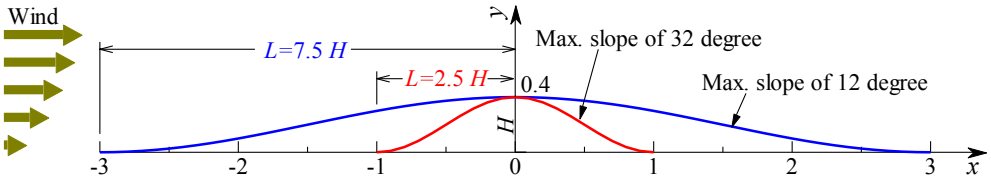


Fig. 4 Two hill shapes

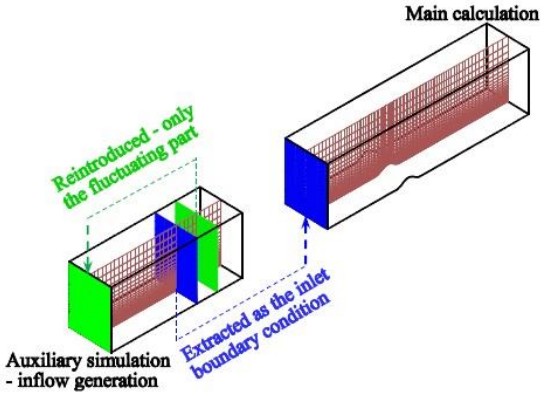


Fig. 5 Two computational domains

The governing equations used for the simulation of flow over the hill, are the three-dimensional unsteady incompressible Navier-Stokes equations in generalized curvilinear coordinate system, shown in tensor form as

$$\begin{cases} \dfrac{\partial (JU_m)}{\partial \xi_m} = 0 \\ J\dfrac{\partial u_i}{\partial t} + \dfrac{\partial (JU_m u_i)}{\partial \xi_m} + \dfrac{1}{\rho}\dfrac{\partial}{\partial \xi_m}\left( J\dfrac{\partial \xi_m}{\partial x_i}\, p \right) = \nu \dfrac{\partial}{\partial \xi_m}\left( JG^{mn}\dfrac{\partial u_i}{\partial \xi_n} \right) \end{cases} \tag{4}$$

where $u_i$ ($i$=1,2,3) are the velocity components $u$, $v$, $w$ in Cartesian coordinate system, respectively; $x_i$ ($i$=1,2,3) are the Cartesian coordinate variables $x$, $y$, $z$, respectively; $t$ = time; $p$ = pressure; $\rho$ = density; $\nu$ = kinematic viscosity coefficient; $\xi_m$ ($m$=1,2,3) are the generalized curvilinear coordinate variables; $U_m$ ($m$=1,2,3) are the contravariant velocity components corresponding to $\xi_m$ ($m$=1,2,3), respectively; $J$ is the Jacobian of the transformation between the physical space and computational space; $G^{mn}$($m$,$n$=1,2,3) is the mesh skewness tensor.

Like the approach to generating inflow turbulence, the fractional step method is also used in the simulation of flow over hills. The governing Eq. (4) are discretized by finite difference scheme with staggered mesh of Maliska's type. In space, a third-order upwind differencing scheme was used for the convective terms while a second-order central differencing scheme was used for the diffusion terms. For time marching, the first-order explicit Euler scheme was used for the unsteady terms, an explicit Adams-Bashforth differencing scheme was applied for the convection terms, and a semi-explicit Crank-Nicolson formulation was applied for the diffusion terms. The computational domain was 40$H$, 15$H$ and 6$H$ in the streamwise, wall-normal and spanwise directions, respectively. The downstream distance from the inlet to the center of the hill was 16.25$H$. The grid system, which had 240, 110, 30 nodes in the streamwise, vertical and spanwise directions, respectively, was fitted to the hill shape, with $\Delta x$=0.05$H$~0.375$H$, $\Delta y$=0.0056$H$~0.495$H$, $\Delta z$= 0.2$H$. The mesh was chosen based on experience, yet not fine enough to resolve the whole wave number range of turbulence. This mesh can ensure $y^+$<1 in calculation for the first layer grid near ground.The CFL number is around 0.41. The mean and turbulence characteristics around the hills were averaged both in time and in the span-wise direction. The averaging was started after the flow reached a stable statistical condition, and the averaging time was 30. The Reynolds number based on the hill height and the averaged upstream wind speed at this height is about 1120.

## 4. Results and discussions

### *4.1 Preservation of inflow turbulence*

We first examine the preservation of inflow turbulence for turbulent inflow case. Figs. 6 and 7 show the turbulence statistics at several positions along the streamwise direction before the steep and low hill, respectively, in which "at inlet" means "at $x/H$=-16.25". The mean-velocity profile and turbulence-intensity profile at the inlet are shown at every selected positions for comparison. For the steep hill, the turbulence statistics preserves well from the inlet to $x/H$=-8, while from $x/H$=-8 to the windward foot of the hill ($x/H$=-2.5), the discrepancy increases gradually because of the obstacle of the steep hill. Clearly, before the steep hill, the mean velocity reduces near ground

and increases in the outer region, and the turbulence intensity increases in the vertical direction, especially in the inner region.Whereas for the low hill, the turbulence statisticspreserves very well for the inlet to $x/H$=-9.27, and only a little discrepancy found at the foot of the hill. Detailed discussion on effects of slope will be given in subsequent sections. From the above, the inflow turbulence imposed at the inlet boundary preserved well in the computational domain for both hills, which forcefully confirms the advantages of the CFD method, in contrast to the artificial method, for generating inflow turbulence.

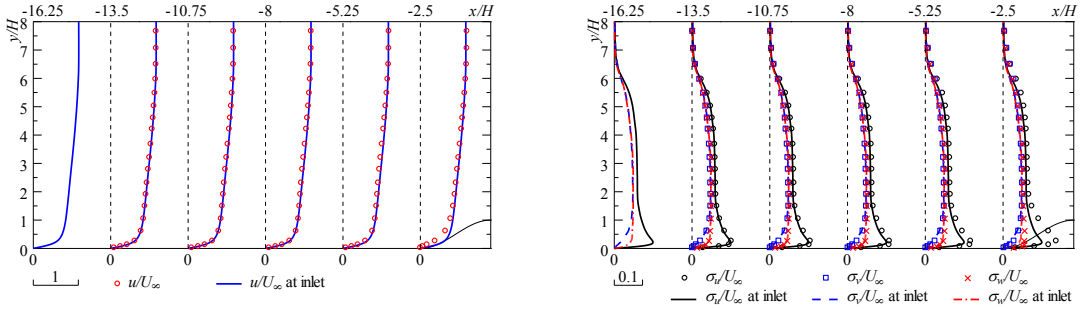


(a)Mean velocity (b)Turbulence intensity

Fig. 6 Variation of turbulence statistics along the streamwise direction before the steep hill

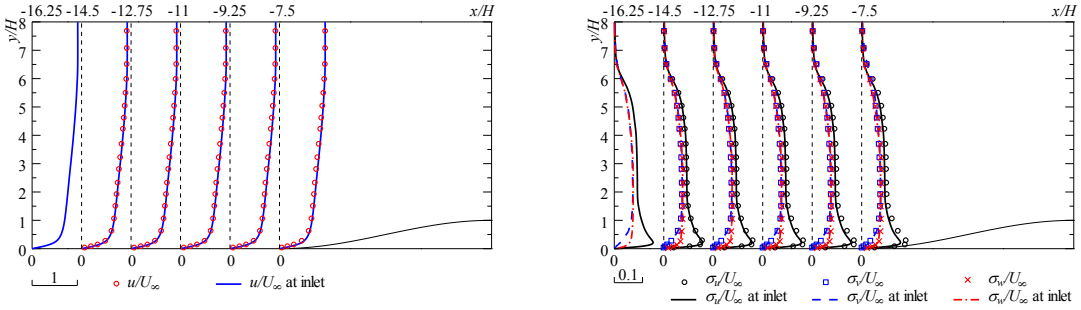


(a)Mean velocity (b)Turbulence intensity

Fig. 7 Variation of turbulence statistics along the streamwise direction before the low hill

### *4.2 Instantaneous flow field*

Now look at the turbulent flow field to examine its unsteady flow features. Figs. 8 and 9 show the 3D view of the flow field over the steep and low hill, respectively. The instantaneous velocity vector in the vertical section and streamwise velocity contour at $y^+$=18, for laminar inflow case and turbulent inflow case, are compared. It is clear that the wake flows for the two hills and two inflow cases are all three-dimensional.Also, the streak like structure can be found before the steep and low hills with turbulent inflow, which means that the generated turbulent flow has reached fully-developed state.From the velocity contours, it can be seen that the velocity near the ground reduces before the hill, increases gradually along the upslope, and reaches the amplitude near the peak.For

the steep hill with laminar in flow shown in Fig. 8(a), there exists an obvious recirculation before the hill, in contrast to the low hill with laminar inflow shown in Fig. 9(a).The recirculation zone behind the hill is smaller under turbulent inflow condition than under turbulent inflow condition for both hills, except that the recirculation zone of the low hill with turbulent inflow is much more smaller (almost vanishes) and discontinuous in spanwise direction.

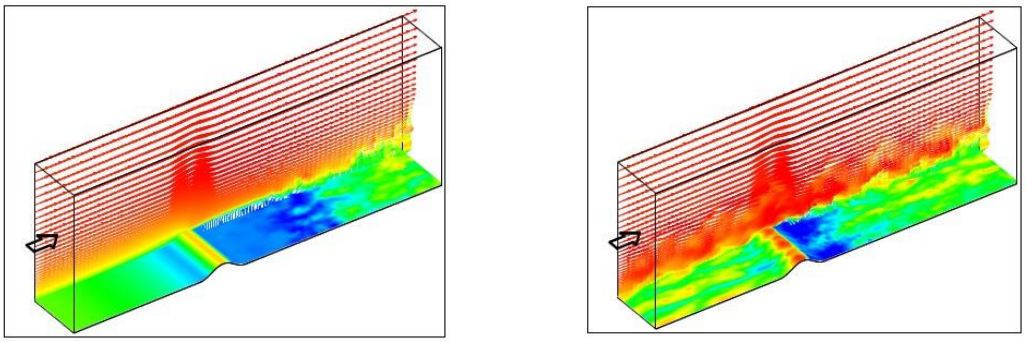

(a) Laminar inflow (b) Turbulent inflow

Fig. 8 3Dview of flow field over the steep hill

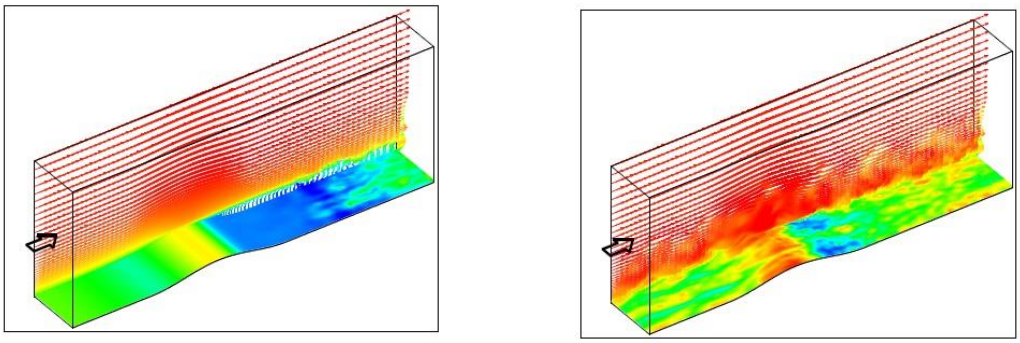

(a) Laminar inflow (b) Turbulent inflow

Fig. 9 3Dview of flow field over the low hill

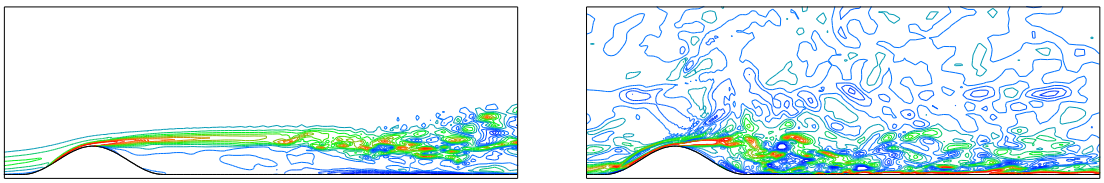

(a) Laminar inflow (b) Turbulent inflow

Fig. 10 Contours of the instantaneous vorticity magnitude over the steep hill

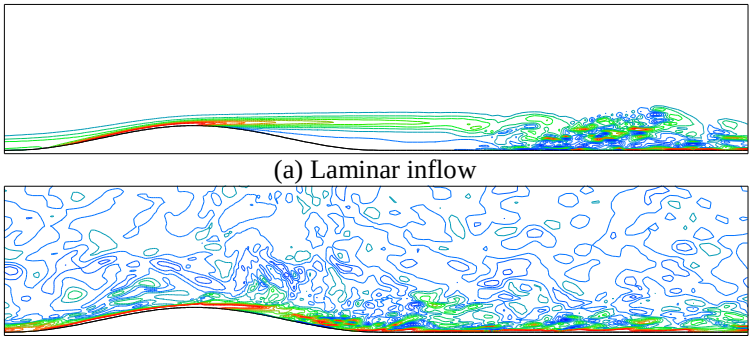

(a) Laminar inflow

(b) Turbulent inflow

Fig. 11 Contours of the instantaneous vorticity magnitude over the low hill

Figs. 10 and 11 show the 2D view of the flow field over the steep and low hill, respectively. The streamwise velocity contour at the central section in spanwise direction, for laminar inflow case and turbulent inflow case, are compared. Obviously, the separated shear layer under turbulent inflow condition reattaches the ground earlier than that under laminar inflow condition. The interaction between the oncoming turbulence and the separated shear layer is the main reason that can be considered for this discrepancy. Figs. 8 and 9 also show that, in the turbulent inflow case,the separated shear layer is disturbed and interrupted, while in the laminar inflow case,the separated shear layer spread downstream more freely. In Fig. 10(a), there is an apparent roll-up of the shear layer behind the steep hill forming a large-scale structure, while in Fig. 10(b), the roll-up structure is much smaller. For the low hill, there is also an apparent and stable separated shear layer under laminar inflow condition just as shown in Fig. 11(a). However, there is no apparent and stable separated layer under turbulent inflow condition as shown in Fig. 11(b). Inflow turbulence can, obviously, increase the turbulence intensity around hills. The steep hill has relatively stronger effects on the flow. There are dense and complex vortices behind the steep hill in contrast to those behind the low hill.

### *4.3 Separation bubble*

The reattachment point or the length of the flow recirculation zone downstream of a hill is of interest for basic understanding of the separation and reattachment behavior and for wind engineering applications. In this study, we investigate the variation of mean reattachment location with the inflow condition and slope.The mean reattachment point is determined to be the location where the spanwise-averaged mean velocity $U$=0 at the nearest grid point to the wall. Fig. 12 compares the time-averaged streamlines of the steep hill for laminar inflow case and turbulent inflow case. A large separation bubble formed behind the steep hill for laminar inflow case, in contrast to the small one for turbulent inflow case. In Fig. 12(a), the horizontal length of the bubble from the separation point to the reattachment point is 13$H$, while in Fig. 12(b), it is 5.5$H$. Besides, a little bubble formed at the foot of the windward slope of the steep hill with laminar inflow, while it almost vanished under turbulent inflow condition. However, for the low hill, there is no separation bubble before the hill, as shown in Fig. 13. The separation bubble behind the low hill with laminar inflow, shown in Fig. 13(a), was also very large, with length of 15.5$H$, longer but

a little thinner than that of the steep hill with laminar inflow shown in Fig. 12(a), while for the turbulent inflow case, this bubble became much smaller and thinner (almost vanished), with length of 4.2*H*, and moved onto the lee slope. The separation point over the hill moves upstream from low hill to steep hill, while moves down stream fromlaminar inflow to turbulent inflow.

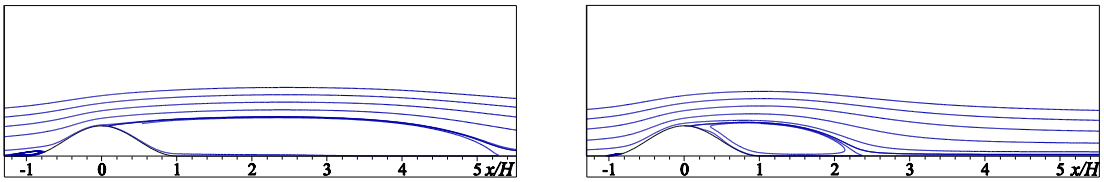


(a) Laminar inflow (b) Turbulent inflow

Fig. 12 Time-averaged streamlines over the steep hill

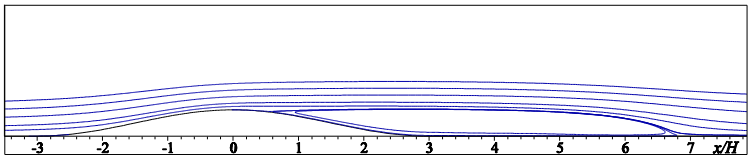


(a) Laminar inflow

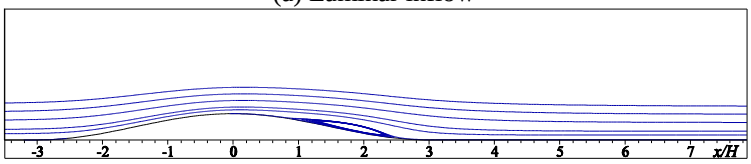


(b) Turbulent inflow

Fig. 13 Time-averaged streamlines over the low hill

### *4.4 Turbulence statistics*

Finally, we focus on the turbulence statistics. Figs. 14 and 15 show the computed mean velocity and *rms* profiles at several positions along the streamwise direction respectively over the steep and low hill under laminar and turbulent inflow conditions, compared with experimental data of Cao *et al.* (2012) at Re=5000 under turbulent inflow condition. Clearly as shown in Fig. 14(a), the mean velocity profiles at turbulent inflow case agree fairly well with experimental data though the experimental Reynolds number is much larger than the numerical one (around 1100). However, the corresponding discrepancy of *rms* is remarkable as shown in Fig. 14(b). The reason may due to the damping function applied in generating inflow turbulence, which overestimates the turbulence intensity near ground as shown in Fig. 2(b). From Fig. 14(a), the flow accelerates on the upslope of the steep hill and much more at the hill crest, and the speedup over the hill under turbulent inflow condition is larger than that under laminar inflow condition. The discrepancy of mean velocity under two different inflow conditions is larger behind the hill than before the hill because of the impacts of separation. Mean reversed flow can be seen leeward of the hill, forming a separation bubble as shown in Fig. 12. From Fig. 14(b), obviously and reasonably, the turbulence intensity under turbulent inflow condition is larger than that under laminar inflow condition, but the discrepancy behind the hill is larger than that before the hill also because of the impacts of

separation. Turbulent intensity has a maximum value near the hill height, corresponding to the location of separated shear layer.An area with large velocity shear and high turbulence intensity at the hill wake, corresponding to the flapping of the separated shear layer, can be seen. The wind characteristics at a large downstream area are influenced by the presence of the hill. Turn to the low hill as shown in Fig. 15. Similar conclusions as those of the steep hill can be concluded except that the velocity shear and turbulence intensity at the hill wake, the reversed flow behind the hill and the affect region of the low hill are smaller.

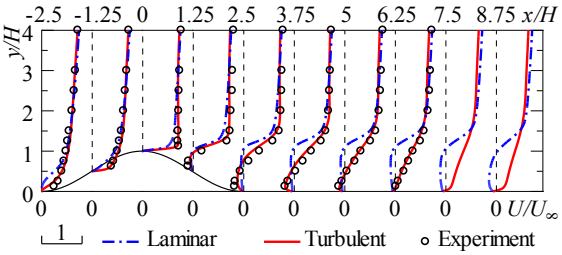


(a) Mean velocity

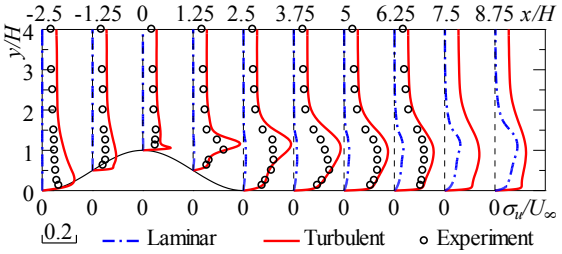


(b) Turbulence intensity

Fig. 14 Turbulent statistics over the steep hill

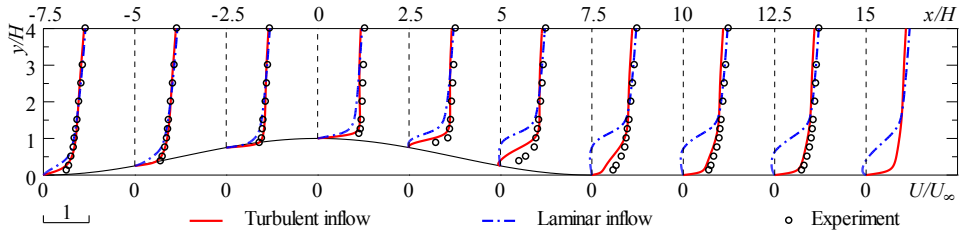


(a) Mean velocity

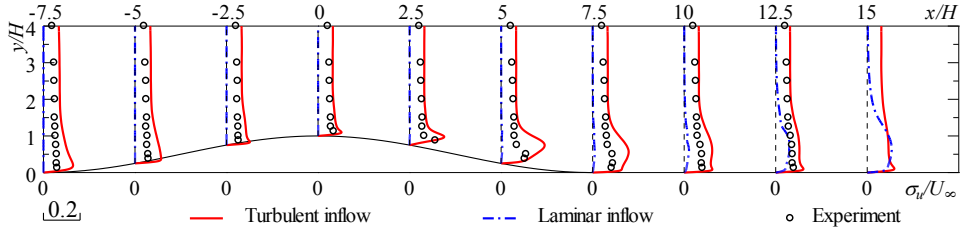


(b) Turbulence intensity

Fig. 15 Turbulent statistics over the low hill

## 5. Conclusions

We performed numerical simulations to study the neutrally stratified turbulent boundary layer over two-dimensional hills with different inflow conditions. Two representative hill shapes with or without stable separation and two representative inflow conditions, laminar and turbulent, were considered. Inflow turbulence was generated by incorporating the local differential quadrature method with the recycling technique, with the effect to improve the high-frequency energy of inflow turbulence. Results show that the imposed inflow turbulence preserved very well in the computational domain. Instantaneous flow data show a stable separated shear layer on the leeside of the steep hill with laminar inflow, while the reattachment point moves upstream under turbulent inflow condition because of the interaction between the oncoming turbulence and the separated shear layer. There is also a stable separated shear layer on the leeside of the low hill with laminar inflow, while no stable and apparent separated layer found in the turbulent inflow case. The time-averaged streamlines show that a small bubble formed at the foot of the windward slope of the steep hill with laminar inflow, while almost vanished under turbulent inflow condition. And there is no separation bubble before the low hill. The separation bubble on the leeside of the low hill under turbulent inflow condition moves onto the lee slope and becomes even smaller than that of the steep hill under the same inflow condition. Turbulence statistics show that the speedup over hills with turbulent inflow is larger than that with laminar inflow. The turbulence intensity under turbulent inflow condition is larger than that under laminar inflow condition, but the discrepancy behind the hill is larger than that before the hill because of separation. In contrast to the steep hill, the velocity shear and turbulence intensity at the hill wake, reversed flow and the affect region of the low hill are smaller. However, the present calculation is carried out withoutany turbulence model to consider SGS stress, and only a low Reynolds number around 1100 is simulated. In our future work, the turbulence model will be incorporated to raise the simulated Reynolds number, and the Reynolds number effect will also be studied.

## Acknowledgments

The research described in this paper was financially supported by the National Natural Science Foundation of China (Grant No. 91215302 and 51278366).

## References

Bitsuamlak, G.T., Stathopoulos, T. and Bédard, C. (2004), "Numerical evaluation of wind flow over complex terrain: review", *J. Aerospace Eng.*, **17**(4), 135-145.

Blocken, B., Stathopoulos, T. and Carmeliet, J. (2007), "CFD simulation of the atmospheric boundary layer: wall function problems", *Atmos. Environ.*, **41**(2), 238-252.

Cao, S. and Tamura, T. (2006), "Experimental study on roughness effects on turbulent boundary layer flow over a two-dimensional steep hill", *J. Wind Eng. Ind. Aerod.*, **94**(1), 1-19.

Cao, S. and Tamura, T. (2007), "Effects of roughness blocks on atmospheric boundary layer flow over a two-dimensional low hill with/without sudden roughness change", *J. Wind Eng. Ind. Aerod.*, **95**(8), 679-695.

Cao, S., Wang, T., Ge, Y. and Tamura, Y. (2012), "Numerical study on turbulent boundary layers over two-

dimensional hills - effects of surface roughness and slope", *J. Wind Eng. Ind. Aerod.*, **104-106**, 342-349.
DeGraaff, D.B. and Eaton, J.K. (2000), "Reynolds-number scaling of the flat-plate turbulent boundary layer", *J. Fluid Mech.*, **422**, 319-346.
Finnigan, J.J. (1988), *Air flow over complex terrain*, (Eds. Steffen, W.L. and Denmead, O.T.), Flow and Transport in the Natural Environment: Advances and Applications, Springer-Verlag, Heidelberg.
Gong, W., Taylor, P.A. and Dornbrack, A. (1996), "Turbulent boundary-layer flow over fixed aerodynamically rough two-dimensional sinusoidal waves", *J. Fluid Mech.*, **312**, 1-37.
Henn, D.S. and Sykes, R.I. (1999), "Large-eddy simulation of flow over wavy surfaces", *J. Fluid Mech.*, **383**, 75-112.
Hunt, J.C.R., Leibovich, S. and Richards, K.J. (1988), "Turbulent shear flow over low hills", *Q. J. Roy. Meteor. Soc.*, **114**(484), 1435-1470.
Ishihara, T. and Hibi, K. (2002), "Numerical study of turbulent wake flow behind a three-dimensional steep hill", *Wind Struct.*, **5**(2-4), 317-328.
Jackson, P.S. and Hunt, J.C.R. (1975), "Turbulent wind flow over a low hill", *Q. J. Roy. Meteor. Soc.*, **101**(430), 929-955.
Kataoka, H. (2008), "Numerical simulations of a wind-induced vibrating square cylinder within turbulent boundary layer", *J. Wind Eng. Ind. Aerod.*, **96**(10-11), 1985-1997.
Kataoka, H. and Mizuno, M. (2002), "Numerical flow computation around aeroelastic 3D square cylinder using inflow turbulence", *Wind Struct.*, **5**(2-4), 379-392.
Kondo, K., Murakami, S. and Mochida, A. (1997), "Generation of velocity fluctuations for inflow boundary condition of LES", *J. Wind Eng. Ind. Aerod.*, **67-68**, 51-64.
Lun, Y.F., Mochida, A., Murakami, S., Yoshino, H. and Shirasaw, T. (2003), "Numerical simulation of flow over topographic features by revised k-ε models", *J. Wind Eng. Ind. Aerod.*, **91**(1-2), 231-245.
Mason, P.J. and King, J.C. (1985), "Measurements and predictions of flow and turbulence over an isolated hill of moderate slope", *Q. J. Roy. Meteor. Soc.*, **111**(468), 617-640.
Miller, C.A. and Davenport, A.G. (1998), "Guidelines for the calculation of wind speed-ups in complex terrain", *J. Wind Eng. Ind. Aerod.*, **74-76**, 189-197.
Neff, D.E. and Meroney, R.N. (1998), "Wind-tunnel modeling of hill and vegetation influence on wind power availability", *J. Wind Eng. Ind. Aerod.*, **74-76**, 335-343.
Ngo, T.T. and Letchford, C.W. (2009), "Experimental study of topographic effects on gust wind speed", *J. Wind Eng. Ind. Aerod.*, **97**(9-10), 426-438.
Tamura, T., Cao, S. and Okuno, A. (2007), "LES study of turbulent boundary layer over a smooth and a rough 2D hill model", *Flow. Turbul. Combust.*, **79**(4),405-432.
Wang, T., Cao, S. and Ge, Y. (2013), "Generation of inflow turbulence using the local differential quadrature method", *J. Wind Eng. Ind. Aerod.*, **122**, 96-104.

*CC*